Functional Connectivity Imaging Analysis: Interhemispheric Integration in Autism

Daniel J. Kelley

Abstract

The human brain connectome is intrinsically organized into small world networks. The network topology of brain can be investigated using anatomical, functional, and effective connectivity. Here we review modern functional connectivity statistics used to examine brain integration. We then assess transcallosal integration in autism during face processing using an interhemispheric partial correlation analysis and a symmetric template registration technique that takes into account the asymmetry of homologous brain regions. Individuals with autism exhibit interhemispheric overconnectivity in both the insula and superior temporal gyrus during face processing when compared to controls.

Introduction

The human brain connectome exhibits intrinsic anatomical and functional brain organization [1-3]. The network topography of human brain can be studied using anatomical, functional, and effective statistical analyses of images collected using a variety of in vivo imaging techniques. Networks of brain function can be understood using functional MRI (fMRI) by examining the segregation of localized activity or the integration of brain regions that form a network [4]. Statistical mapping of brain function using fMRI traditionally focused on the magnitude of segregated activity during task-specific paradigms. Localized activation within the brain was first detected with fMRI using product moment correlation [5,6] which was used as an index of association between the recorded fMRI signal at each voxel and a task design vector. As an alternative to mapping segregated patterns of localized brain activation using correlation, information transfer within the brain can be investigated by examining the integration of BOLD responses among brain regions using functional connectivity imaging analysis.

Functional Connectivity

Functional connectivity, the "temporal correlations between remote physiological events" [7] is a means by which information integrated between and within brain regions can be detected. However, for some functional connectivity studies, the definition also includes correlations across subjects [8] or correlations of segregated activations (beta weights) across event types [9]. Functional connectivity is distinct from effective connectivity, "the influence one neuronal system exerts over another" [10]. Effective connectivity requires an *a priori* model for causal relationships, unlike functional connectivity which is considered to be more exploratory in nature [11]. Functional connectivity, unlike effective connectivity, neither presumes a causal connection between regions nor explains the driving force of interregional correlations. In the context of connectivity analysis, correlation and regression are not comparable because regression has a causal interpretation. In fact, regression can be considered the simplest structural equation model, an effective connectivity technique. Functional connectivity using fMRI was first applied to the motor cortex of resting human brain using the product moment correlation of BOLD time courses [12,13]. Temporal functional connectivity techniques vary with experimental design. Block design studies are able to utilize the variance at the beginning and end of a block for connectivity analysis and condition specific block connectivity is possible using simple subtraction to separate blocks. As the stimulus presentation shortens to that of an event-related design, measuring connectivity for specific trial conditions becomes more difficult since the individual trial signal variance is masked by the overlapping hemodynamic response functions of adjacent trials [14]. Functional connectivity measures can be tested for significance using random field theory [15]. The integrity of functional connectivity between nodes determines the extent of integration of circuits in the functional network.

Functional connectivity can be examined during tasks or at rest [16] and analyzed using univariate and multivariate[17] techniques that take the form of correlations among time series using temporal and frequency based approaches [18] or the spectral decomposition of time series into their spatial modes [15]**.** In this report, we review functional connectivity

statistics and outline an interhemispheric connectivity analysis using partial correlations to examine transcallosal integration in autism.

Functional Connectivity Statistics

Bravais-Pearson product moment correlation

The **Bravais-Pearson product moment correlation** in fMRI analysis can be defined as:

$$r = r_{xy} = \frac{s_{xy}}{s_x s_y} = \frac{\sum_{i=1}^{n} x_i y_i}{\sqrt{\sum_{i=1}^{n} x_i^2 \sum_{i=1}^{n} y_i^2}};\ s_{xy} = \frac{\sum_{i=1}^{n} (x_i - \bar{x})(y_i - \bar{y})}{(n-1)}$$

where s_x and s_y are the sample standard deviations, $\bar{x}$ and $\bar{y}$ are the sample means based on n time series measurements of random variables X and Y [19]. Rather than using this index as a measure of association between the recorded fMRI signal at each voxel and a task design vector [5,6,20], this statistic can also be used for connectivity analysis [12,13] and to determine the number of edges and distances between nodes in a theoretical graph framework [21]. The correlation coefficient, used as a functional connectivity measure, can be derived from LSE regression, an effective connectivity measure, via the equation [22]:

$$r^2 = \beta_{xy}\, \beta_{yx}$$

where β_{xy} and β_{yx} are the coefficients for regressing x on y and y on x respectively. This equation identifies the squared correlation of functional connectivity as the interaction between effective connectivity weights with exchanged dependent and independent variables. One disadvantage of product-moment correlation is that the sampling distribution of non-zero correlations is skewed. This can be corrected using the nonlinear Fisher r to z' transformation [23]:

$$z' = \frac{\ln(1+r) - \ln(1-r)}{2} \quad \text{or} \quad z' = \tanh^{-1}(r)\ ;\ sd_{z'} = \frac{1}{\sqrt{n-3}}$$

The linear correlation can be tested using [24,25]:

$$t = r\frac{\sqrt{n-2}}{\sqrt{1-r^2}};\ df = n-2$$

For seed correlation analyses, t-transformed correlations of Gaussian smoothed time series form a t-field and can be tested for significance on a t-distribution; however, cross-correlation, autocorrelation, and homologous correlation fields do not from a t-field when t-transformed so tests of significance need to be based on random field theory [15,26]. Thresholded correlations are a useful statistic to detect functional connectivity in local networks but may be less useful localizing long range networks compared to PCA and SVD discussed below [27]. Another disadvantage is that the product moment correlation only describes linear association. The **generalized correlation** coefficient is a correntropy statistic based on mutual information that captures both linear and non-linear contributions, unlike Pearson's correlation, and does so preserving the sign of the correlation measure unlike canonical correlation [28]. Curvilinear relations can be assessed using the **index of correlation**, r_{yx} [29]:

$$r_{yx} = \frac{\sigma_{\hat{y}}}{\sigma_y}$$

where $\sigma_{\hat{y}}$ is the standard deviation of the estimates for y, $\hat{y}$, when y is regressed on x, and σ_y is the standard deviation of the actual y values.

Intraregional Connectivity Analysis: COSLOF Index

The cross-correlation coefficients of spontaneous low frequency synchrony (COSLOF index) was originally developed to identify alterations in hippocampal functional synchrony due to neurodegeneration in Alzheimer disease [30]. As an estimate of intraregional connectivity, the COSLOF index serves as a metric for functional synchrony within a region of interest. The COSLOF index is generated by:

$$COSLOF = \frac{2}{K(K-1)} \sum_{i,\, j=1, i>j}^{K} cc_{ij}$$

where K is the number of voxels and cc_{ij} is the cross-correlation coefficient between the ith and jth voxel time course in the ROI. Reductions or increases in the COSLOF index would be interpreted as dysfunctional connectivity. While originally developed for resting state connectivity, a COSLOF-like index representing the average cross correlation coefficient within a region of interest may serve equally well as a functional

connectivity index during an event-related task. The disadvantage of this technique is that it is restricted to linear associations since it is based on Pearson's correlation.

Beta Series Correlation Analysis

Beta series correlation analysis (BSCA) operates within the general linear model to estimate beta values for individual events as an estimate of BOLD response magnitude. These parameter estimates for each trial can be categorized to produce a beta series for each trial type. The BSCA multivariate approach is distinct from more typical univariate approaches in that variability of individual trials is taken into account with the former, but not the latter, method [9]. The collection of beta series within an ROI can then be used as seeds in a voxelwise correlation analysis. This technique has been validated with coherence measures of connectivity on a previously published dataset and applied in a working memory study investigating functional connectivity with the fusiform face area during a delayed face recognition task [31]. The disadvantage of this technique is that it is essentially a correlation of regression estimates and is less robust than a structural equation modeling approach.

Real-time Connectivity Analysis

Real-time functional connectivity analyses have applications in behavioral therapy as a biofeedback mechanism. Predictive models are able to forecast future connectivity estimates and would give subjects feedback closer to real-time. Examples of forecasting estimates include mean absolute deviation, Theil's U-statistic, and state-space models [32]. Dynamic linear models are state space models using Bayesian inference, have applications in real-time analyses, and have the form:

$$Y = X \Theta + v$$

where Y is the dependent variable vector, X is the independent variable vector, Θ is an unknown parameter vector, and v is an error vector. Online correlation, principal component (PCA), independent component (ICA), and entropy analyses are methods to evaluate connectivity features of the brain in real-time [33]. Online correlation analysis in particular is easily implemented (see Appendix) and is useful for observing the evolution

of the correlation coefficient over time, but does not take into account non-linear associations.

Asymmetric Functional Connectivity Analysis

Although no anatomical constraints are required in functional connectivity analysis, anatomical constraints may be useful in identifying asymmetric chronoarchitecture. One measure of asymmetric functional connectivity is the **laterality index** which has the form:

$$\text{Laterality Index} = \frac{L - R}{L + R}$$

where L is left hemisphere activation and R is activation in the corresponding region of the right hemisphere [34,35]. A disadvantage of the laterality index is that its application is limited to functional systems whose anatomical connections are asymmetric. An alternative statistic is the **spatial coincidence coefficient** (SCC) for contralateral connectivity [36]:

$$SCC_{LR} = SCC_{RL} = \frac{2n_{LR}}{2n_L n_R + n_{LO} + n_{RO}}$$

This statistic is useful for determining the extent of asymmetric functional connectivity using Pearson's correlation based on the mean number of voxels above threshold in the right ROI (R), in the left ROI (L), or outside either ROI (O). A disadvantage of this technique is that it is threshold dependent, although it was originally developed as a means to estimate an appropriate threshold in resting state networks by penalizing undesirable connectivities.

Rank Correlations

Rank correlation coefficients are non-parametric measures of similarity that can be implemented by converting the fMRI time series to ranks. The most well known non-parametric correlation statistic is the **quadrant correlation**, also known as Blomqvist's q statistic or the medial correlation statistic [37]. The quadrant correlation is the sample correlation between the signs of deviations from the median and has the form [22,38]:

$$r_Q = \frac{1}{n}\sum sign\left[(x_i - median(x))(y_i - median(y))\right]$$

Spearman rank correlation, r_s, can be rewritten using the difference in ranks $d_i = x_i - y_i$ using the equation:

$$r_s = 1 - \frac{6\sum_{i=1}^{n} d_i^2}{N(N^2 - 1)}$$

However, when the proportion of tied ranks is large, a correction factor, T, is required:

$$r_s = 1 - \frac{(N^3 - N) - 6\sum_{i=1}^{n} d_i^2 - (T_x + T_y)/2}{\sqrt{(N^3 - N)^2 - (T_x + T_y)(N^3 - N) + T_x T_y}};\ T = \sum_{i=1}^{g}(t_i^3 - t_i)$$

where r_s is the Spearman rank correlation with correction for tied ranks, g is the number of different tied rank groupings, and t_i is the number of tied ranks in the *i*th grouping [19]. A disadvantage of the Spearman correlation is that it's significance testing can only be approximated [39]. The Spearman correlation is closely related to Pearson's correlation and can be converted to a product moment correlation using Pearson's approximation [40]:

$$\rho_s = \frac{6}{\pi}\sin^{-1}\left(\frac{1}{2}\rho\right)$$

Kendall's rank order correlation or Kendall's tau, τ , is an alternative statistic that quantifies the disagreement of rankings in X and Y and has the form:

$$\tau = \frac{4P}{n(n-1)} - 1$$

where P is the total number of agreements [41]. With tied ranks, the equation becomes:

$$\tau = \frac{P - Q}{\sqrt{\left[n(n-1)/2\right] - K_x}\sqrt{\left[n(n-1)/2\right] - K_y}};\ K_x = \frac{1}{2}\sum f_i(f_i - 1)$$

where f_i is the number of tied observations in each group of ties on X and

$$K_y = \frac{1}{2}\sum f_i(f_i - 1)$$

where f_i is the number of tied observations in each group of ties on Y. In practice, a general rule for non-parametric tests is for n <30 use Spearman's correlation if there are

no expected differences in ranks or outliers; otherwise, Kendall's correlation is preferred. For n> 30, either Spearman's or Kendall's correlation is acceptable [39], however, Spearman's coefficient may perform better that Kendall for a large n and is easier to calculate [42]. The Spearman or Kendall coefficients can be z-tested for significance after a Fisher r to z conversion [24].

Partial Correlation

Partial correlation is used to measure the association between two time series, A and B, after the effects of other time series are partialed out from both A and B [24,43]. If three time series are involved and a multivariate normal distribution is assumed, the sample estimate for the Pearson partial correlation coefficient $\rho_{12.3}$ can be defined as:

$$r_{12.3} = \frac{r_{12} - r_{13}r_{23}}{\sqrt{(1-r_{13}^2)(1-r_{23}^2)}}$$

Yule generalized the partial correlation to n time series as follows [44]:

$$r_{12.34\ldots n} = \frac{r_{12.34\ldots(n-1)} - r_{1n.34\ldots(n-1)}r_{2n.34\ldots(n-1)}}{(1-r_{1n..34\ldots(n-1)}^2)^{1/2}(1-r_{2n.34\ldots(n-1)}^2)^{1/2}}$$

The Pearson partial correlation is usually smaller than the product-moment correlation unless a covariate of no interest is present that is highly correlated with the predictors but uncorrelated with the dependent variable [45]. **Kendall's partial tau correlation** has the form:

$$\tau_{12\cdot3} = \frac{(\tau_{12} - \tau_{13}\tau_{23})}{\left[(1-\tau_{13}^2)(1-\tau_{23}^2)\right]^{1/2}}$$

Where τ_{12}, τ_{13}, and τ_{23} are Kendall's rank correlations[46]. Kendall also described a partial correlation for **Spearman's partial correlation** and suggested this approach could only be defended by analogy with Kendall's partial correlation:

$$\rho_{23.1} = \frac{\rho_{23} - \rho_{12}\rho_{13}}{(1-\rho_{12}^2)^{1/2}(1-\rho_{13}^2)^{1/2}}$$

where $\rho_{23.1}$ is the partial correlation between variables 2 and 3 when variable 1 is constant. The partial correlation can be tested on a t-distribution:

$$t = r_{xy.1\ldots q}\frac{\sqrt{n-q-2}}{\sqrt{1-r^2_{xy.1\ldots q}}};\ df = n-q-2$$

where q is the number of variable partialled out [47].

Semipartial and Multiple Semipartial Correlation

A **semipartial correlation**, also known as a part correlation, quantifies the relationship between time series A and B after partialing out other time series from A but not B. The partial correlation is greater than or equal to the semipartial correlation and can be determined from the multiple correlation discussed below [43]. The **multiple semipartial correlation** quantifies the correlation of A with B and C and the effects of other variables are removed from B and C. Both the squared semipartial and squared multiple semipartial correlation can be determined from the difference of squared multiple correlations[43]. The advantage of these correlations is that specific network interactions can be assessed. The disadvantage is that only linear effects are modeled.

Multiple Correlation

The **multiple correlation** coefficient, R, is the product moment correlation between a time series, A, and the estimated time series from multiple regression when regressing A on the linear combination of remaining time series [41]. In the multiple regression framework, the squared multiple correlation $R^2_{Y.1,\ldots,J}$ can be interpreted as the proportion of variance in the dependent variable explained by the independent variables [48]:

$$R^2_{Y.1,\ldots,J} = \frac{SS_{regression}}{SS_{total}}$$

Multiple correlation is the maximum correlation possible between the dependent variable and the linear combination of independent variables [43]. There is discrepancy whether the

multiple correlation statistic should be reported as squared, i.e. as the coefficient of multiple determination, [48] or not [49]. The sample multiple correlation can be adjusted to account for its overestimation of the population multiple correlation [48] and can be tested on the F-statistic [47]:

$$F(J, n-J-1) = \frac{R^2_{Y.1,\ldots,J}}{1-R^2_{Y.1,\ldots,J}} * \frac{n-J-1}{J}$$

Partial Multiple Correlation

The partial multiple correlation, also known as multiple partial correlation, quantifies the linear relationship between a dependent variable and a group of independent variables after partialling out another group of variables from both the independent and dependent variables [43,50,51]. The squared **partial multiple correlation** has the form:

$$R^2_{a.b(c)} = \frac{R^2_{a.bc} - R^2_{a.c}}{1-R^2_{a.c}}$$

Where $R^2_{a.b(c)}$ is the squared partial multiple correlation between variable a and dependent variables in b [x1,x2,x3…xn] while partialing out the control variables in c [z1,z2,…,zn] from both a and b, $R^2_{a.bc}$ is the squared multiple correlation between the dependent variable a and all other variables in b and c, i.e. [x1,…,xn,z1,…,zn], and $R^2_{a.c}$ is the multiple correlation between the independent variable a and control variables in c [43]. The basic difference between a partial and partial multiple correlation is the number of independent variables. The partial correlation has one independent variable but the partial multiple correlation has more than one independent variable [43].

Comparison of Part, Partial, and Multiple Correlations

In the context of time series, multiple and partial correlation work best when the form of multiple regression is linear [52]. Multiple and partial correlation are distinct [53]. Multiple correlation is used to determine the relation between a given time series and all other time series; whereas, partial correlation characterizes the relation between two time series while controlling for all additional time series [44]. In partial correlation, each variable in

the correlation is residualized on the variables of no interest. This is in contrast to the semipartial correlation statistic in which the correlation is between an unmodified variable and a variable residualized on one or more other variables. The squared semipartial correlation statistic can be calculated by subtracting the squared multiple correlation between the dependent variable and variables of no interest from the squared multiple correlation between the dependent variable and all independent variables [43]. The advantage of these techniques is that multiple connectivity patterns can be modeled; however, these patterns are only modeled in a linear fashion.

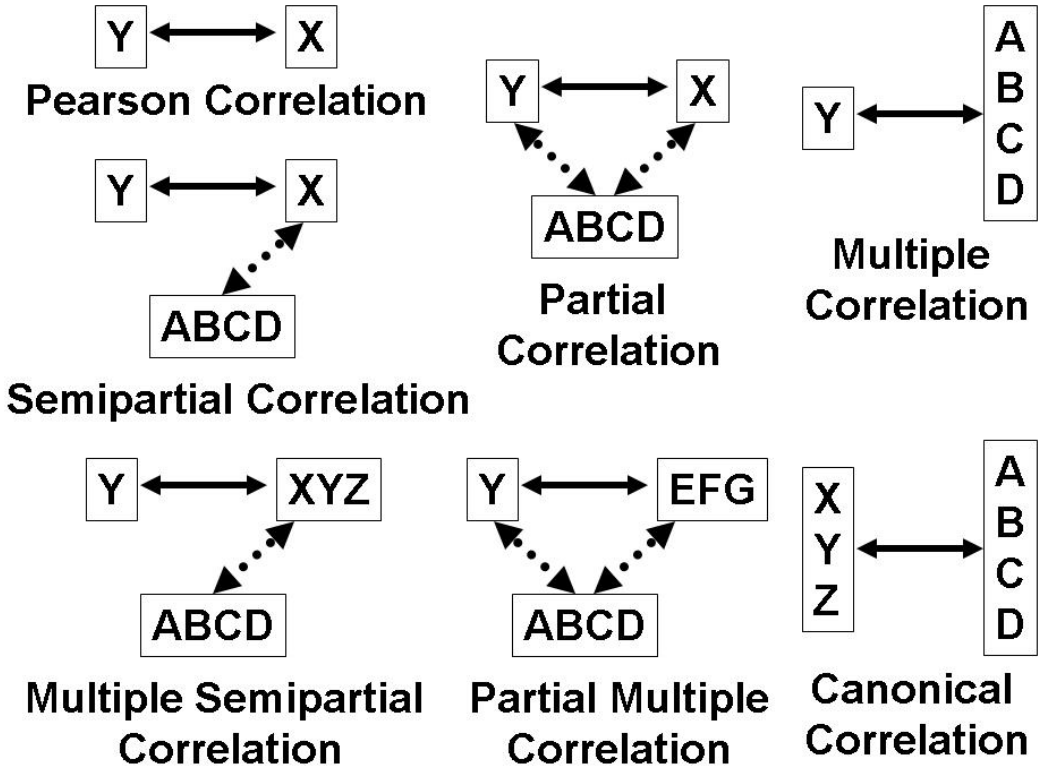

Figure 1: Correlations for Functional Connectivity

Canonical Correlation

The canonical correlation[54] is a multivariate statistic that measures the overall strength of interrelationships between a set of multiple dependent variables and a set of multiple independent variables [55]. Calculating the canonical correlation involves the maximization of the correlation between set X and set Y, each of which contains variables representing

timeseries from separate voxels [56]. The canonical correlation can be derived by analogy with multiple regression and multiple correlation [57] and has the form:

$$| R_{yy}^{-1} R_{yx} R_{xx}^{-1} R_{xy} - \lambda I | = 0$$

where | | denotes the determinant, R_{yy} is the correlation matrix of the variables in set Y, R_{xx} is the correlation matrix of variables in set X, R_{xy} is the correlation matrix of set X variables with set Y variables, R_{yx} is the transpose of R_{xy}, λ are the eigenvalues, and I is the identity matrix. The canonical correlation, R_c, varies between 0 and 1 and is the correlation between the two canonical variates, the weighted linear combination of each set that maximizes R_c and has the form [43]:

$$R_c = \sqrt{\lambda}$$

The canonical variates are the results from a canonical variates analysis [58]. As indicated by this equation, canonical correlation does not provide directionality of the correlation unlike the Pearson correlation [28]. The maximum number of canonical correlations corresponds to the lowest number of variables in either set X or Y. Subsequent pairs of canonical variates are orthogonal to all prior pairs and produce canonical correlations with decreasing magnitude. The square of the canonical correlation represents the variance shared by each pair of canonical variates in X and Y. Multiple regression is a type of canonical analysis in which only one dependent variable is present [43]. The canonical correlation statistic is useful in functional connectivity because, unlike multiple regression, the canonical correlation is symmetric in the sense that either set could be the dependent or independent set and still produce the same result [59]. Canonical variates analysis can be used in a multivariate framework to identify patterns of task dependent The canonical correlation can be used to formulate Wilk's lambda [43]:

$$\Lambda = (1 - R_{c_1}^2)(1 - R_{c_2}^2)\ldots(1 - R_{c_j}^2)$$

Where Λ is Wilk's lambda, $R_{c_1}^2$ is the square of the first canonical correlation, $R_{c_2}^2$ is the square of the second canonical correlation, and $R_{c_j}^2$ is the square of the jth canonical

correlation. The significance of the canonical correlation can be tested using Wilk's lambda directly using random field theory [60] or using Bartlett's significance test of lambda using the chi-squared distribution:

$$\chi^2 = -[N - 1 - 0.5(p + q + 1)]\ln(\Lambda);\ df = pq$$

where N is the number of subjects; p is the number of variables on the left; q is the number of variables on the right; and df is the degrees of freedom [43]. Correction of the maximum or principal canonical correlation for multiple comparisons can be determined using random field theory [61]. A difficulty with canonical correlation is that it is sensitive to multicollinearity.

Time Dependent Regression Estimation

Dynamic changes in connectivity are not accounted for by the stationary and constant network estimates [62,63]. Variable parameter regression models beta variation and has the form[64]:

$$y_t = x_t\beta_t + u_t$$

$$u_t \sim N(0, \sigma^2);\ t = 1, \ldots, T$$

Variable parameter regression with Kalman filtering models the time-varying parameter estimate using a random walk [65] . A disadvantage of the Kalman filter is that it is a one sided filtering technique that requires estimation of the initial state. A preferred approach in the economics literature is Schlicht's method for variable parameter regression which uses a two-sided filter that makes no assumptions about the initial state and uses all the time points to estimate each coefficient [66]. Alternatively, partly conditional time varying coefficient modeling estimates regression parameters as a function of predicted and predictor variable timing using an extension of marginal regression analysis [67]. These methods may be useful to observe the task-dependent changes in fMRI connectivity studies and are comparable to the psychophysiological interaction analyses discussed below.

Psychophysiological Interaction (PPI)

Rather than estimating the beta weight as a random walk over time, the beta coefficient could be estimated as a function of time-dependent explanatory variables [65]. A **psychophysiological interaction** refers to a change in the slope, when regressing activity from two brain regions, brought about by a psychological variable [68]. PPI enables the determination of the contribution that activity in a given brain region is influenced by the interaction between a psychological variable and the activity of another brain region [69]. Activity in PPI analysis is modeled using three explanatory regressors including a voxel time course as the physiological, brain response variable; a psychological variable based on the context of the stimuli presented [70]; and the psychophysiological product of the former two variables [11,71]. The first two regressors are treated as regressors of no interest and the third is used to generate statistical maps. In other words, this analysis can identify a region, A, of brain that is active in response to a stimulus only when another region, B, of brain is active. The interpretation would be that region B's activity modulates the activity of region A indicating they are effectively connected [68]. However large number of inputs to a region are required to interpret results in the context of effective connectivity; and, signal from one ROI can only be interpreted in the context of functional connectivity [68,71]. This may be one reason why PPI analysis has been categorized as a functional connectivity technique [11]. Unlike functional connectivity analysis, PPI provides insight into the directionality of the "contextual modulation of connectivity," because the statistical maps generated depend upon which physiological node in the functional circuit was used to generate the psychophysiological interaction regressor [72].

Fractal Connectivity

Fractals are self-similar patterns that follow a power law of the form:

$$N = s^{d}$$

where d is the fractal dimension. The term fractal is derived from Latin meaning broken. The term fractal in fractal dimension describes the "broken" non-integer nature of d and

dimension refers to the power law relationship that defines the self-similarity property [73]. Fractal analysis methods to determine the fractal dimension include the Hausdorff, Minkowski-Bougliand, calliper, box counting, and mass-radius methods [74]. The fractal dimension of a given time series can be assessed using a dispersion method based on the standard deviation [75]:

$$SD(m=1) = \frac{1}{N}\sqrt{N\sum_{i=1}^{N} x^2(i) - [\sum_{i=1}^{N} x(i)]^2}$$

This calculation is then repeated for a new time series that has adjacent points averaged and N/2 points to determine SD(m=2), and with 4 points averaged to produce SD(m=4), until the number of total points is less than 4. The slope of a log SD(m) vs log m plot can then be subtracted from 1 to quantify the fractal dimension[75], which can be interpreted as a measure of internal or self-similar connectivity. Fractal networks of brain connectivity exhibit small world properties that can be assessed using measures of degree, the clustering coefficient, and the minimum path length [76]. Fractals have the advantage of characterizing networks across several levels of complexity; however, fractal analysis of real data, unlike mathematical constructs, may not have adequate sensitivity to characterize subtle differences in complexity which rarely has more self-similarity than two orders of magnitude [74].

Wavelet Correlation

Wavelets are fractal functions that take into account the 1/f, long memory properties of the BOLD response and, for this reason, wavelet analysis is preferred to simple correlation analysis as an estimator of functional connectivity [77]. The wavelet coefficients produced from decomposition of each time series can be used to calculate the **wavelet correlation coefficient** which is derived from the ratio of wavelet covariances and variances [78,79] and has the form [23]:

$$\rho_x(\lambda_j) = \frac{\gamma_x(\lambda_j)}{\sigma_1(\lambda_j)\sigma_2(\lambda_j)};\ \gamma_x(\lambda_j) = \frac{1}{2\lambda_j} Cov(w_{1,j,t}, w_{2,j,t})$$

where $\gamma_x(\lambda_j)$ is the covariance of ($x_{1,t}$,$x_{2,t}$) for scale λ_j; $w_{1,j,t}$ and $w_{2,j,t}$ are the scale λ_j wavelet coefficients for $x_{1,t}$ and $x_{2,t}$; and $\sigma_1(\lambda_j)$ and $\sigma_2(\lambda_j)$ are the wavelet variances

for x1,t and x2,t . Wavelet correlation has an advantage over other correlation procedures because this statistic integrates both phase and amplitude information and overcomes the difficulties of window width selection [80]. Further development of the wavelet correlation using the MODWT, maximal overlap discrete wavelet transform, can be found in its application to small world properties of low frequency neural fluctuations [81]. A Matlab toolbox has also been developed (see Appendix).

Coherence Analysis

Event-related fMRI integration can be examined using coherence, a frequency based correlation measure [82,83]. More specifically, **coherence** is defined as:

$$Coherence_{xy}(g) = \left|R_{xy}(g)\right|^2 = \frac{\left|f_{xy}(g)\right|^2}{f_{xx}(g)\,f_{yy}(g)}$$

where $R_{xy}(g)$ is the complex valued coherency of time series x and y, $f_{xy}(g)$ is the cross-spectrum of x and y, and $f_{yy}(g)$ is the power spectrum of y. An advantage of coherence analysis is that functional connectivity can be measured independent of HRF form and independent of hemodynamic spatial heterogeneity. A disadvantage of this technique is that the temporal waveforms of condition specific trial types are unable to be separated due to overlapping hemodynamics of adjacent event-related trials. Task dependent changes in coherence over time may be detectable using time-varying transfer functions[84].

Spectral Decomposition Methods

For further elaboration of the techniques discussed below and significance testing, the reader is referred to a recent review[85,86].

Eigenimage or spatial mode analysis

Functional connectivity can be measured with eigenimage analysis using singular value decomposition [87,88]. **Singular value decomposition** is a method of data reduction that is

applicable to canonical correlation and principal component analysis [89] and decomposes a matrix into orthonormal bases using [90];

$$A = UDV^T$$

where A is a scan time by brain voxel matrix containing BOLD signal intensities; U is a time by eigenvoxel matrix whose orthonormal columns contain the left singular vectors, temporal eigenvectors, or eigenvariates; D is an eigenvoxel by eigentime diagonal matrix of singular values in A which, when squared, are the eigenvalues that indicate eigenintensity; and V is a voxel by eigentime matrix whose orthonormal columns are the right singular vectors, spatial eigenvectors, or eigenimages [91,92].

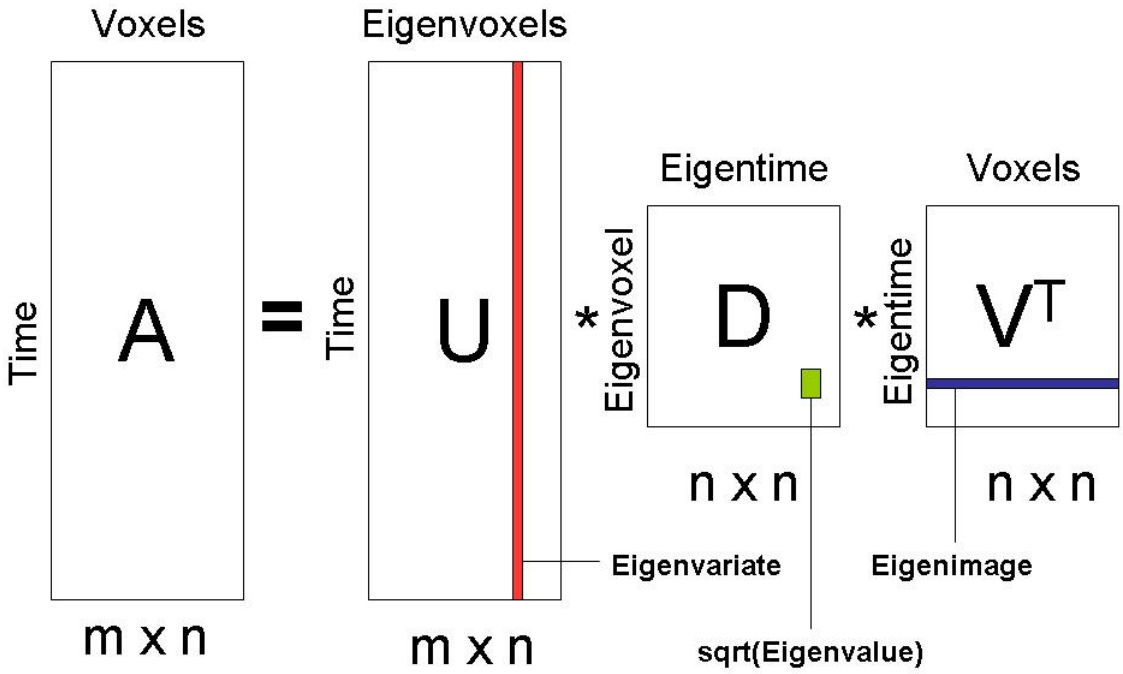

Figure 2: Singular Value Decomposition, adapted from [90]

Each eigenimage, or spatial mode, in V is a voxel-dependent profile of each eigenvariate and defines a functionally connected, but distributed, brain system; and, each eigenvariate

in U is a time-dependent profile of each eigenimage [87]. **Generalized eigenimage analysis** can be used to identify group differences in eigensystems:

$$C_j d = C_i d\lambda$$

where C is the correlation matrix of groups i and j and d is the generalized eigenimage [87]. A disadvantage of these these techniques is that they are sensitive to preprocessing and significant results can only be characterized descriptively[86].

Multidimensional Scaling

Metric **multidimensional scaling**, or principal coordinates analysis, is a multivariate technique to visualize functional connectivity by mapping anatomy into functional space[93] and takes the form:

$$AA^T = U\lambda U^T;\ X = A^T U$$

Using MDS, singular value decomposition of the correlation matrix, AA^T, produces eigenvectors in U used to determine the location of voxels in functional space, X. The distance between nodes derived with MDS can be related to the correlation coefficient [94]:

$$d_{ij} = \sqrt{2}\sqrt{(1-\rho_{ij})}$$

where d is the distance between nodes i and j, and ρ_{ij} is the correlation of time series x_i and y_j. A disadvantage of this technique is that the graphical display restricts the number of data points that can be plotted and too many points make interpretation difficult.

Principle and Independent Component Analysis

PCA and ICA are exploratory methods in functional connectivity [86] that can be implemented using SVD [92]. The key difference between PCA and ICA analysis is that PCA identifies uncorrelated, Gaussian source signals but ICA identifies sources that are non-Gaussian and independent [92]. Principle component analysis (PCA) can give insight into functionally connected spatial modes by identifying the orthogonal axes producing maximal signal variance [88]. In principal components analysis, the covariance matrix of the data, is used to produce the eigenimages in V unlike eigenimage analysis which uses the data matrix itself or MDS which uses the correlation matrix [88,95]. ICA approaches are

considered data driven and do not require an a priori model which makes them especially useful for identifying resting state networks [16]. The application of either spatial or temporal independent component analyses to functional connectivity depends on the task and hypothesis [96]. In functional connectivity analysis, an advantage of ICA is that it is not dependent on voxel seed, unlike simple correlation, and is robust to structured noise; but, the bases may not fully characterize the networks and the resulting maps are difficult to threshold [97]. Nonlinear ICA and PCA techniques attempt to overcome the orthogonal and linear drawbacks of eigenimage analysis [87].

Partial Least Squares

Partial least squares is a multivariate regression technique that predicts the dependent variable set from the independent variable set by maximizing the covariance between the decomposed sets of dependent and independent variables [98]. Partial least squares was implemented in fMRI analysis using the single value decomposition of a covariance matrix between brain images and a behavioral or task design [99]. Rather than applying the SVD to a correlation or covariance matrix of identical brain images as with eigenimage analysis and MDS [99], PLS uses the covariance matrix of two different sets of images to investigate connectivity between brain systems [87]. In the context of interhemispheric connectivity, PLS can identify systems of connectivity within a hemisphere that have the greatest connectivity between hemispheres:

$$A_i^T A_j = UDV^T ;\ D = U^T M_i^T M_j V$$

where the columns of U and V contain the singular images and the diagonal matrix, D, contains the singular values which represent the extent of functional connectivity between the two hemispheres, i and j [94]. Partial least squares is fundamentally different from canonical variates analysis because PLS optimizes covariance patterns but CVA optimizes canonical variate correlations [99]. The main disadvantages for PLS are the potential for inconsistent parameter estimation[100], difficulty interpreting independent latent variable loadings, and the need to bootstrap for significance testing[101].

Information Theory Approaches

Mutual information and entropy are statistics in information theory that can be applied to functional connectivity analysis. **Mutual information**, MI, measures the information about X contained in Y or vice versa since mutual information is a symmetric function [102]:

$$MI(X,Y) = H(X) + H(Y) - H(X,Y)$$

where differential entropy is:

$$H(X) = -\int_X p(x)\log_2(p(X))dX$$

Entropy is a measure of information gain over time [103,104] and cross-entropy is a non-linear method to assess the complexity of interaction between time series [75].
Friston and colleagues [94] showed that mutual information between two time series from voxels p and q can be written in terms of the correlation coefficient

$$MI_{pq} = -\log(1-\rho^2)/2$$

An advantage of mutual information over simple correlation is that mutual information can be extended to multivariate assessment. For example, when determining the relationship between multiple time series from region p and q, mutual information can be written as [94]:

$$MI_{pq} = \log\left(\left[\frac{\left|A_p^T A_p\right| * \left|A_q^T A_q\right|}{\left[A^T A\right]}\right]^{\frac{1}{2}}\right)$$

A disadvantage of mutual information is that it does not differentiate between positive and negative associations like Pearson's correlation[105] but has the advantage of being able to identify relations between p and q that lack dependence, unlike Pearson's correlation[106].

Conclusion

Functional networks can be mapped in subjects at rest or performing tasks using fMRI functional connectivity analyses. Both univariate and multivariate statistical approaches

are available to identify human chronoarchitecture in specific functional circuits or whole networks respectively. Functional connectivity analysis is centered on the spectral decomposition of time series or temporal associations in the time and frequency domain. Time series analysis in the time, frequency, or fractal domains may be conducted across voxels, clusters, or groups of individuals. Functional connectivity analysis techniques are no longer just "temporal correlations" and may require a revision of Friston's original definition of functional connectivity that adequately characterizes newer approaches such as fractal, coherence, and beta series correlation approaches.

Case Study:

Transcallosal Face Integration in Autism

Dan Kelley, Kim Dalton, Moo Chung, Richard Davidson
Waisman Laboratory for Brain Imaging and Behavior; University of Wisconsin-Madison.

Introduction

Functional connectivity studies are being used to clarify the role of corpus callosum anatomy on transcollosal integration. The extent of transcallosal integration varies among individuals and shows a dependence on task complexity [107]. Theories for interhemispheric integration include asymmetric interhemispheric inhibition, information transfer, and hemispheric recruitment [108]. The corpus callosum has several roles and its role in interhemispheric inhibition is known to increase through development [109]. Interhemispheric information transfer depends on an intact corpus callosum based on studies of split brain and corpus callosum agenesis patients [110]. A functional connectivity study of corpus callosum agenesis identified the presence of intrahemispheric connectivity, but mostly absent interhemispheric connectivity measures, during auditory and motor tasks [111]. Behavioral studies suggest interhemispheric transfer of emotional information is a function of emotional significance [112], that interhemispheric processing increases the accuracy of face and facial expression matching [113], and that emotional faces have an interhemispheric processing advantage over neutral faces [114]. Multimodal approaches using fMRI connectivity and DTI indicate that the relationship between

corpus callosum integrity and network integration can influence behavior [115]. As an effective connectivity measure, dynamic causal models are useful in identifying context-dependent changes in reciprocal interhemispheric connections between homotopic brain regions [116].

Autism is a neurodevelopmental disorder with a classic triad of deficits in the social, behavioral and communicative domain that may be due to complex connectivity alterations in both brain structure and function [117]. Both anatomical and functional measures indicate that transcallosal integration is altered in autism. After controlling for brain volume, gender, and performance IQ, the volume of the body and splenium were reduced in autism [118] using an adaptation of the Wittelson scheme [119]. A 2D voxel-based morphometric analysis of midsagittal corpus callosum identified reductions in autism genu and splenium white matter density after controlling for age [120]. Reduced fractional anisotropy measures using diffusion tensor imaging are noted in the corpus callosum and indicate that interhemispheric processing is altered [121,122]. Functional connectivity studies also suggest that interhemispheric connectivity is reduced in autism at rest [123] and during sentence comprehension [124], working memory [125], and Tower of London tasks [126].

Interhemispheric functional connectivity analysis between homotopic brain regions, or transcollosal integration analysis (TIA), will provide insight into the functional consequences of callosum alterations in autism. However, TIA is complicated by neuroanatomical asymmetries present in the human brain[127-129]. Identification of homotopic brain regions using manual parcellation is laborious but registration techniques from voxel based morphometry are automated and can account for these asymmetries. Here we describe a functional connectivity approach using partial correlation analysis that accounts for brain asymmetry to examine interhemispheric integration that could contribute to aberrant social behavior in autism.

Methods

Study design and task methodology have been reported elsewhere [130]. Briefly, twelve male control subjects with a mean age (+/- SD) of 17.0 (+/- 2.86) and twelve males with

autism or Asperger's disorder aged 16.75 (+/- 4.52) years were recruited from a list of available autism volunteers maintained at the University of Wisconsin-Madison Waisman Center. Ages were not significantly different [t(22) = -0.162, P = 0.87] between groups. Criteria for diagnosing autism and Asperger's Disorder included DSM-IV and confirmation with the Autism Diagnositic Interview Revised (ADI-R). Subjects participated in an event-related fMRI study using a facial emotion recognition task. In total 40 faces, 16 neutral and 24 emotional (8 happy, 8 fear, 8 anger), from the Karolinska Directed Emotional Faces Set [131] were presented for 3 seconds each with a jittered inter-trial interval ranging from 5 to 7 seconds. Subjects were instructed to decide if the face displayed an emotion (happy, fear, anger) or was neutral and to indicate their choice with a button box press. Both accuracy (percent correct) and reaction times were measured. Image acquisition consisted of 409 gradient recalled echo-planar images using BOLD contrast (TE = 30 ms; TR = 2 sec; FOV = 240x240 mm, 64x64 matrix, voxel size= 3.75 x 3.75 x 5mm) acquired sagittally (30 slices. 4mm thick with 1mm gap) with a 3.0 Tesla GE SIGNA Scanner (Waukesha, WI). Axial T1-weighted 3D SPGR images were also acquired (TE = 8 ms, TR = 35 ms, FOV = 240x240 mm, 256x192 matrix, 124 axial slices, slice thickness = 1.1-1.2 mm, NEX = 1, flip angle = 30 degrees). Analyses were carried out using AFNI[132] and software developed in house. Echoplanar images were filtered in the spatial frequency domain, reconstructed, motion corrected, and registered to anatomical data. Two group level analyses between Autism (n=12) and Controls (n=12) were conducted. The first analysis was conducted in Talairach space (AFNI) which preserved brain asymmetries. In this approach, all anatomical for autism and control subjects were corrected for non-uniformities and brought into Talairach space after manual marker placement. The second analysis was conducted in a symmetric Talairach space to take into account anatomical asymmetries and was based on a voxel based morphometry asymmetry analysis[127]. Manually Talairached anatomical images were averaged across all subjects in both groups. A symmetric template was generated by mirroring the mean anatomical image about the midline anterior-posterior plane. Each subject's anatomical image was automatically registered to the symmetric template using a 12 parameter affine transform. In both analyses, each subject's functional image underwent the same transformation as the corresponding anatomical image. We used the

partial correlation between a brain volume and the identical volume mirrored about the midline anterior-posterior plane as the TIA statistic and partialled out physiological noise using the mean whole brain time course [133]. The partial correlation statistic was converted to a z-score and group differences were determined with a 2-tailed t-test. The same binary mask of mean brain volume downsampled to functional resolution was applied to results in both analyses. In both analyses, we tested the null hypothesis that mean transcallosal integration was comparable between autism and controls.

Results

The symmetric template accounted for asymmetric differences in brain anatomy as evident in the posterior portions of Figure 1. A t-test identified a group interhemispheric connectivity difference in the insula which was more integrated in autism With both the symmetric and asymmetric template, we detected group differences in insula connectivity that was more integrated in autism (Figures 2 and 3). Using the symmetric template, we were also able to detect a group difference in connectivity between the superior temporal gyri which was greater in autism that was unable to be detected with the asymmetric template (Figure 4).

Conclusion

In this paper we describe differences in autism information transfer using fMRI and a voxelwise whole brain interhemispheric functional connectivity analysis we call transcallosal integration analysis. During face processing, the insulae were significantly more connected in autism and interinsular projections are carried by the callosum. In monkeys, interhemispheric fibers of the insula cross in the ventral portion of the corpus callosum and are topographically organized with rostral insula fibers crossing in the rostral corpus callosum body and caudal insula traveling through caudal portions of the corpus callosum body [134]. We also visually compared two methods to determine whether brain asymmetries affect transcallosal integration analysis. In this case study, TIA using the asymmetric or symmetric template adequately detected the primary group difference in interhemispheric insula connectivity. However, smaller clusters of significant interhemispheric connectivity between superior temporal gyri were only detectable with

the symmetric Talairach template (Figure 4). Symmetric templates may be useful in correcting for asymmetries in functional connectivity among smaller regions at the group level. Given that the spatial heterogeneity of hemodynamic response functions (HRFs) complicates estimation of functional connectivity between heterotopic brain regions [135,136], our transcallosal integration approach has the advantage of comparing regions with similar hemodynamic transfer functions based on the similarity of homologous neurovascular architectures. Further studies using more samples will be necessary to assess the utility of symmetric templates in transcallosal integration analyses.

References

1. Ioannides, A. A. Dynamic functional connectivity. *Curr Opin Neurobiol* **17**, 161-70 (2007).
2. Sporns, O. & Honey, C. J. Small worlds inside big brains. *PNAS* **103**, 19219-19220 (2006).
3. Sporns, O., Tononi, G. & Kötter, R. The Human Connectome: A Structural Description of the Human Brain. *PLoS Computational Biology* **1**, e42 (2005).
4. Friston, K. Beyond phrenology: what can neuroimaging tell us about distributed circuitry? *Annu Rev Neurosci* **25**, 221-50 (2002).
5. Bandettini, P. A., Wong, E. C., Hinks, R. S., Tikofsky, R. S. & Hyde, J. S. Time course EPI of human brain function during task activation. *Magn Reson Med* **25**, 390-7 (1992).
6. Bandettini, P. A., Jesmanowicz, A., Wong, E. C. & Hyde, J. S. Processing strategies for time-course data sets in functional MRI of the human brain. *Magn Reson Med* **30**, 161-73 (1993).
7. Friston, K. J. (1994).
8. Zald, D. H., Donndelinger, M. J. & Pardo, J. V. Elucidating dynamic brain interactions with across-subjects correlational analyses of positron emission tomographic data: the functional connectivity of the amygdala and orbitofrontal cortex during olfactory tasks. *J Cereb Blood Flow Metab* **18**, 896-905 (1998).
9. Rissman, J., Gazzaley, A. & D'Esposito, M. Measuring functional connectivity during distinct stages of a cognitive task. *Neuroimage* **23**, 752-63 (2004).
10. Friston, K. J., Frith, C. D. & Frackowiak, R. S. J. Time-dependent changes in effective connectivity measured with PET. *Human Brain Mapping* **1**, 69-79 (1993).
11. Dodel, S. et al. Condition-dependent functional connectivity: syntax networks in bilinguals. *Philos Trans R Soc Lond B Biol Sci* **360**, 921-35 (2005).
12. Biswal, B., Yetkin, F. Z., Haughton, V. M. & Hyde, J. S. Functional connectivity in the motor cortex of resting human brain using echo-planar MRI. *Magn Reson.Med.* **34**, 537-541 (1995).

13. Biswal, B. B., Van, K. J. & Hyde, J. S. Simultaneous assessment of flow and BOLD signals in resting-state functional connectivity maps. *NMR Biomed.* **10**, 165-170 (1997).
14. Buchel, C. Perspectives on the estimation of effective connectivity from neuroimaging data. *Neuroinformatics.* **2**, 169-174 (2004).
15. Worsley, K. J., Cao, J., Paus, T., Petrides, M. & Evans, A. C. Applications of random field theory to functional connectivity. *Hum Brain Mapp* **6**, 364-7 (1998).
16. Damoiseaux, J. S. et al. Consistent resting-state networks across healthy subjects. *PNAS* **103**, 13848-13853 (2006).
17. Abdi, H. in *Encyclopedia for research methods for the social sciences* (ed. M. Lewis-Beck, A. B., T. Futing) 699-702 (Sage, Thousand Oaks, CA, 2003).
18. Salvador, R. et al. Frequency based mutual information measures between clusters of brain regions in functional magnetic resonance imaging. *NeuroImage* **35**, 83-88 (2007).
19. Marques de Sa, J. *Applied Statistics Using SPSS, STATISTICA, and Matlab* (Springer-Verlag, Berlin, 2003).
20. Friman O, Borga M, Lundberg P & H., K. in *Proceedings of the 12th Scandinavian Conference on Image Analysis.* (SCIA, Bergen, Norway, 2001).
21. Jiang, T., He, Y., Zang, Y. & Weng, X. Modulation of functional connectivity during the resting state and the motor task. *Hum Brain Mapp* **22**, 63-71 (2004).
22. Shevlyakov, G. L. & Vilchevski, N. O. *Robustness in Data Analysis: Criteria and Methods* (ed. Solotarev, V.) (2002).
23. Gencay, R., Selcuk, F. & Whitcher, B. *An Introduction to Wavelets and Other Filtering Methods in Finance and Economics* (Elsevier, San Diego, CA, 2001).
24. Snedechor, G. W. & Cochran, W. G. *Statistical Methods* (Blackwell Publishing, Ames, IA, 1989).
25. Chung, M. K. in *The Encyclopedia of Measurement & Statistics* 73-74 (Sage Publications, 2007).
26. Cao, J. a. W., K.J. The geometry of correlation fields with an application to functional connectivity of the brain. *Annals of Applied Probability* **9**, 1021-1057 (1999).
27. Worsley, K. J., Chen, J. I., Lerch, J. & Evans, A. C. Comparing functional connectivity via thresholding correlations and singular value decomposition. *Philos Trans R Soc Lond B Biol Sci* **360**, 913-20 (2005).
28. Lange, O. F. & Grubmuller, H. Generalized correlation for biomolecular dynamics. *Proteins* **62**, 1053-61 (2006).
29. Ezekiel, M. *Methods of Correlation Analysis* (John Wiley & Sons, Inc., New York, Ny, 1947).
30. Li, S. J. et al. Alzheimer Disease: Evaluation of a Functional MR Imaging Index as a Marker. *Radiology* **225**, 253-259 (2002).
31. Gazzaley, A., Rissman, J. & Desposito, M. Functional connectivity during working memory maintenance. *Cogn Affect Behav Neurosci* **4**, 580-99 (2004).
32. Yelland, P. M. & Lee, E. in *SML Technical Report Series* (Sun Microsystems, Inc., 2003).
33. Kasabov, N. in *Perspectives in Neural Computing* (ed. Taylor, J.) 143-161 (Springer-Verlag, London, 2003).

34. Tamada, T., Miyauchi, S., Imamizu, H., Yoshioka, T. & Kawato, M. Cerebro-cerebellar functional connectivity revealed by the laterality index in tool-use learning. *Neuroreport* **10**, 325-331 (1999).
35. Dijkhuizen, R. M. et al. Correlation between brain reorganization, ischemic damage, and neurologic status after transient focal cerebral ischemia in rats: a functional magnetic resonance imaging study. *J.Neurosci.* **23**, 510-517 (2003).
36. Biswal, B. B., Van Kylen, J. & Hyde, J. S. Simultaneous assessment of flow and BOLD signals in resting-state functional connectivity maps. *NMR Biomed* **10**, 165-70 (1997).
37. Blomqvist, N. On a Measure of Dependence Between two Random Variables. *The Annals of Mathematical Statistics* **21**, 593-600 (1950).
38. Dehon, C., Algllaf, F., Crouz, C. & Zamar, R. in *International Conference on Robust Statistics* (2005).
39. Masur, H., Papke, K., Althoff, S. & Oberwittler, C. *Scales And Scores In Neurology: Quantification of Neurological Deficits in Research and Practice* (ed. Beall, M.) (Thieme, New York, NY, 2004).
40. Moran, P. A. Rank correlation and Product-Moment Correlation. *Biometrika* **35**, 203-06 (1948).
41. Glass, G. V. & Stanley, J. S. *Statistical Methods in Education and Psychology* (Prentice-Hall, Inc., Englewood Cliffs, NJ, 1970).
42. Zar, J. H. (Pearson Education, Inc., Dehli, India, 1999).
43. Pedhauser, E. J. *Multiple Regression in Behavioral Research Explanation and Prediction* (Holt, Rinehart, and Winston, New York, NY, 1982).
44. Ivy, H. M. *What is the relation of academic preparation, experience, intelligence, achievement, and sex of rural teachers in Mississippi to their pay?* (George Peabody College for Teachers, Nashville, TN, 1922).
45. Schumacker, R. E. & Lomax, R. G. *A Beginner's Guide to Structural Equation Modeling* (Lawrence Erlbaum Asssociates, Inc., Mahwah, New Jersey, 2004).
46. Kendall, M. G. Partial Rank Correlation. *Biometrika* **32**, 277-283 (1942).
47. Neter, J., Wasserman, W. & Kutner, M. H. *Applied Linear Statistical Models: Regression, Analysis of Variance, and Experimental Designs* (Richard D. Irwin, Inc., Homewood, IL, 1985).
48. Abdi, H. in *Encyclopedia of Measurement and Statistics.* (Sage, Thousand Oakes, CA, 2007).
49. Dunteman, G. H. & Ho, M.-H. R. *An Introduction to Generalized Linear Models* (SAGE Publications, 2006).
50. Evans, C. H. (National Academies Press, 2001).
51. Cowden, D. J. The Multiple-Partial Correlation Coefficient. *Journal of the American Statistical Association* **47**, 442-456 (1952).
52. Lawrance, A. J. Partial and Multiple Correlation for Time Series. *The American Statistician,* **33**, 127-130 (1979).
53. Guttman, L. A Note on the Derivation of Formulae for Multiple and Partial Correlation. *The Annals of Mathematical Statistics* **9**, 305-308 (1983).
54. Hotelling, H. Relations Between Two Sets of Variates. *Biometrika* **28**, 321-377 (1936).

55. Joseph F. Hair, J., Anderson, R. E. & Tatham, R. L. *Multivariate Data Analysis with Readings* (Macmillan Publishing Company, New York, 1987).
56. Friman, O., Borga, M., Lundberg, P. & Knutsson, H. in *Proceedings of the SSAB Symposium on Image Analysis* (2001).
57. Cramer, E. M. Note: A simple Derivation of the Canonical Correlation Equations. *Biometrics* **29**, 379-380 (1973).
58. Worsley, K. J., Poline, J. B., Friston, K. J. & Evans, A. C. Characterizing the response of PET and fMRI data using multivariate linear models. *Neuroimage* **6**, 305-19 (1997).
59. Muller, K. E. Understanding Canonical Correlation through the General Linear Model and Principal Components. *The American Statistician* **36**, 342-354 (1982).
60. Carbonell, F., Galan, L. & Worsley, K.J. The geometry of the Wilks's Lambda random field. *Annals of the Institute of Statistical Mathematics* (2005).
61. Worsley, K. J., Charil, A., Lerch, J. & Evans, A.C. in *2005 International Joint Conference on Neural Networks* (Montreal, Quebec, 2005).
62. Cui, Q., Liu, B., Jiang, T. & Ma, S. Characterizing the dynamic connectivity between genes by variable parameter regression and Kalman filtering based on temporal gene expression data. *Bioinformatics* **21**, 1538-1541 (2005).
63. Li, X. et al. Discovery of Time-Delayed Gene Regulatory Networks based on temporal gene expression profiling. *BMC Bioinformatics* **7**, 26 (2006).
64. Jezzard, P., Mathews, P. M. & Smith, S. M. *Functional MRI: An Introduction to Methods* (Oxford University Press, New York, NY, 2005).
65. Buchel, C. & Friston, K. J. Dynamic changes in effective connectivity characterized by variable parameter regression and Kalman filtering. *Hum Brain Mapp* **6**, 403-8 (1998).
66. Schlicht, E. in *Discussion Papers in Economics from University of Munich, Department of Economics.* (Munich, Germany, 2005).
67. Pepe, M. S., Heagerty, P. & Whitaker, R. Prediction Using Partly Conditional Time-Varying Coefficients Regression Models. *Biometrics* **55**, 944-950 (1999).
68. Friston, K. J. et al. Psychophysiological and modulatory interactions in neuroimaging. *Neuroimage.* **6**, 218-229 (1997).
69. Das, P. et al. Pathways for fear perception: modulation of amygdala activity by thalamo-cortical systems. *NeuroImage* **26**, 141-148 (2005).
70. Boksman, K. et al. A 4.0-T fMRI study of brain connectivity during word fluency in first-episode schizophrenia. *Schizophrenia Research* **75**, 247-263 (2005).
71. Egner, T. & Hirsch, J. The neural correlates and functional integration of cognitive control in a Stroop task. *Neuroimage* **24**, 539-47 (2005).
72. Stephan, K. E. On the role of general system theory for functional neuroimaging. *J Anat* **205**, 443-70 (2004).
73. Smith, T. G., Jr., Marks, W. B., Lange, G. D., Sheriff, W. H., Jr. & Neale, E. A. A fractal analysis of cell images. *J Neurosci Methods* **27**, 173-80 (1989).
74. Fernandez, E. & Jelinek, H. F. Use of Fractal Theory in Neuroscience: Methods, Advantages, and Potential Problems. *Methods* **24**, 309-321 (2001).
75. Kuusela, T. A., Jartti, T. T., Tahvanainen, K. U. O. & Kaila, T. J. Nonlinear methods of biosignal analysis in assessing terbutaline-induced heart rate and blood pressure changes. *Am J Physiol Heart Circ Physiol* **282**, H773-781 (2002).

76. Bassett, D. S., Meyer-Lindenberg, A., Achard, S., Duke, T. & Bullmore, E. From the Cover: Adaptive reconfiguration of fractal small-world human brain functional networks. *PNAS* **103**, 19518-19523 (2006).
77. Achard, S. & Bullmore, E. Efficiency and Cost of Economical Brain Functional Networks. *PLoS Comput Biol* **3**, e17 (2007).
78. Whitcher, B., Guttorp, P. & Percival, D. B. Mathematical Background for Wavelet Estimators of Cross-Covariance and Cross-Correlation. *National Research Center for Statistics and the Environment Technical Report Series* **38** (1999).
79. Whitcher, B., Guttorp, P. & Percival, D. B. Wavelet analysis of covariance with application to atmospheric time series. *National Research Center for Statistics and the Environment Technical Report Series* **24** (1999).
80. Kawata, K. & Arimoto, S. Signal Matching Using Wavelet Correlation. *Electronics and Communication in Japan* **79**, 23-34 (1996).
81. Achard, S., Salvador, R., Whitcher, B., Suckling, J. & Bullmore, E. A Resilient, Low-Frequency, Small-World Human Brain Functional Network with Highly Connected Association Cortical Hubs. *J. Neurosci.* **26**, 63-72 (2006).
82. Sun, F. T., Miller, L. M. & D'Esposito, M. Measuring interregional functional connectivity using coherence and partial coherence analyses of fMRI data. *Neuroimage.* **21**, 647-658 (2004).
83. Carter, G. C. Coherence and time delay estimation. *Proceedings of the IEEE* **75**, 236- 255 (1987).
84. Zhao, H., Lu, S., Zou, R., Ju, K. & Chon, K. H. Estimation of time-varying coherence function using time-varying transfer functions. *Ann Biomed Eng* **33**, 1582-94 (2005).
85. Petersson, K. M., Nichols, T. E., Poline, J. B. & Holmes, A. P. Statistical limitations in functional neuroimaging. II. Signal detection and statistical inference. *Philos Trans R Soc Lond B Biol Sci* **354**, 1261-81 (1999).
86. Petersson, K. M., Nichols, T. E., Poline, J. B. & Holmes, A. P. Statistical limitations in functional neuroimaging. I. Non-inferential methods and statistical models. *Philos Trans R Soc Lond B Biol Sci* **354**, 1239-60 (1999).
87. Friston, K. & Buchel, C. in *Statistical Parametric Mapping: The Analysis of Functional Brain Images* (ed. Penny, W. D.) 492-507 (Elsevier, Oxford, UK, 2007).
88. Friston, K. J., Frith, C. D., Liddle, P. F. & Frackowiak, R. S. Functional connectivity: the principal-component analysis of large (PET) data sets. *J Cereb Blood Flow Metab* **13**, 5-14 (1993).
89. Hammarling, S. The singular value decomposition in multivariate statistics. *ACM SIGNUM Newsletter* **20**, 2-25 (1985).
90. Wall, M. E., Rechtsteiner, A. & Rocha, L. M. in *A Practical Approach to Microarray Data Analysis.* (ed. Granzow, M.) 91-109 (Kluwer, Norwell, MA, 2003).
91. Alter, O., Brown, P. O. & Botstein, D. Singular value decomposition for genome-wide expression data processing and modeling. *PNAS* **97**, 10101-10106 (2000).
92. Stone, J. V. *Independent component analysis : a tutorial introduction* (MIT Press, Cambridge, Mass., 2004).

93. Friston, K. J., Frith, C. D., Fletcher, P., Liddle, P. F. & Frackowiak, R. S. J. Functional Topography: Multidimensional Scaling and Functional Connectivity in the Brain. *Cereb. Cortex* **6**, 156-164 (1996).
94. Friston, K. J. Functional and effective connectivity in neuroimaging: A synthesis. *Human Brain Mapping* **2**, 56-78 (1994).
95. Qi, H., Wang, T.-W. & Birdwell, J. D. in *Statistical Data Mining and Knowledge Discovery* (ed. Bozdogan, H.) (CRC Press, Boca Raton, Florida, 2004).
96. Calhoun, V. D., Adali, T., Pearlson, G. D. & Pekar, J. J. Spatial and temporal independent component analysis of functional MRI data containing a pair of task-related waveforms. *Hum Brain Mapp* **13**, 43-53 (2001).
97. Ma, L., Wang, B., Chen, X. & Xiong, J. Detecting functional connectivity in the resting brain: a comparison between ICA and CCA. *Magnetic Resonance Imaging* **25**, 47-56 (2007).
98. Abdi, H. in *Encyclopedia for research methods for the social sciences* (ed. M. Lewis-Beck, A. B., T. Futing) 792-795 (Sage, Thousand Oaks, CA, 2003).
99. McIntosh, A. R., Bookstein, F. L., Haxby, J. V. & Grady, C. L. Spatial pattern analysis of functional brain images using partial least squares. *Neuroimage* **3**, 143-57 (1996).
100. Cassel, C., Hackl, P. & Westlund, A. H. Robustness of partial least-squares method for estimating latent variable quality structures. *Journal of Applied Statistics* **26**, 435-446 (1999).
101. Garson, G. D. (http://www2.chass.ncsu.edu/garson/pa765/statnote.htm, 2007).
102. Deleus, F. F. D. M., P.A. Van Hulle, M.M. in *Proceedings of the 2002 12th IEEE Workshop on Neural Networks for Signal Processing* 119 - 128 (2002).
103. de Araujo, D. B. et al. Shannon entropy applied to the analysis of event-related fMRI time series. *NeuroImage* **20**, 311-317 (2003).
104. Tedeschi, W. et al. Generalized mutual information tests applied to fMRI analysis. *Physica A: Statistical Mechanics and its Applications* **352**, 629-644 (2005).
105. Steuer, R., Kurths, J., Daub, C. O., Weise, J. & Selbig, J. The mutual information: Detecting and evaluating dependencies between variables. *Bioinformatics* **18**, S231-240 (2002).
106. Priness, I., Maimon, O. & Ben-Gal, I. Evaluation of gene-expression clustering via mutual information distance measure. *BMC Bioinformatics* **8**, 111 (2007).
107. Belger, A. & Banich, M. T. Costs and benefits of integrating information between the cerebral hemispheres: a computational perspective. *Neuropsychology* **12**, 380-98 (1998).
108. Stephan, K. E., Marshall, J. C., Penny, W. D., Friston, K. J. & Fink, G. R. Interhemispheric Integration of Visual Processing during Task-Driven Lateralization. *J. Neurosci.* **27**, 3512-3522 (2007).
109. Hoptman, M. J. & Davidson, R. J. How and why do the two cerebral hemispheres interact? *Psychol Bull* **116**, 195-219 (1994).
110. Paul, L. K. et al. Agenesis of the corpus callosum: genetic, developmental and functional aspects of connectivity. *Nat Rev Neurosci* **8**, 287-99 (2007).
111. Quigley, M. et al. Role of the corpus callosum in functional connectivity. *AJNR Am J Neuroradiol* **24**, 208-12 (2003).

112. Compton, R. J., Wilson, K. & Wolf, K. Mind the gap: interhemispheric communication about emotional faces. *Emotion* **4**, 219-32 (2004).
113. Compton, R. J. Inter-hemispheric interaction facilitates face processing. *Neuropsychologia* **40**, 2409-19 (2002).
114. Compton, R. J., Feigenson, K. & Widick, P. Take it to the bridge: an interhemispheric processing advantage for emotional faces. *Brain Res Cogn Brain Res* **24**, 66-72 (2005).
115. Baird, A. A., Colvin, M. K., Vanhorn, J. D., Inati, S. & Gazzaniga, M. S. Functional connectivity: integrating behavioral, diffusion tensor imaging, and functional magnetic resonance imaging data sets. *J Cogn Neurosci* **17**, 687-93 (2005).
116. Stephan, K. E., Penny, W. D., Marshall, J. C., Fink, G. R. & Friston, K. J. Investigating the functional role of callosal connections with dynamic causal models. *Ann N Y Acad Sci* **1064**, 16-36 (2005).
117. Rippon, G., Brock, J., Brown, C. & Boucher, J. Disordered connectivity in the autistic brain: challenges for the "new psychophysiology". *Int J Psychophysiol* **63**, 164-72 (2007).
118. Piven, J., Bailey, J., Ranson, B. & Arndt, S. An MRI study of the corpus callosum in autism. *Am J Psychiatry* **154**, 1051-1056 (1997).
119. Witelson, S. F. Hand and sex differences in the isthmus and genu of the human corpus callosum. A postmortem morphological study. *Brain* **112 (Pt 3)**, 799-835 (1989).
120. Chung, M. K., Dalton, K. M., Alexander, A. L. & Davidson, R. J. Less white matter concentration in autism: 2D voxel-based morphometry. *Neuroimage* **23**, 242-51 (2004).
121. Keller, T. A., Kana, R. K. & Just, M. A. A developmental study of the structural integrity of white matter in autism. *Neuroreport* **18**, 23-7 (2007).
122. Alexander, A. L. et al. Diffusion tensor imaging of the corpus callosum in Autism. *Neuroimage* **34**, 61-73 (2007).
123. Horwitz, B., Rumsey, J. M., Grady, C. L. & Rapoport, S. I. The cerebral metabolic landscape in autism. Intercorrelations of regional glucose utilization. *Arch Neurol* **45**, 749-55 (1988).
124. Just, M. A., Cherkassky, V. L., Keller, T. A. & Minshew, N. J. Cortical activation and synchronization during sentence comprehension in high-functioning autism: evidence of underconnectivity. *Brain* **127**, 1811-21 (2004).
125. Koshino, H. et al. Functional connectivity in an fMRI working memory task in high-functioning autism. *Neuroimage* **24**, 810-21 (2005).
126. Just, M. A., Cherkassky, V. L., Keller, T. A., Kana, R. K. & Minshew, N. J. Functional and Anatomical Cortical Underconnectivity in Autism: Evidence from an fMRI Study of an Executive Function Task and Corpus Callosum Morphometry. *Cereb. Cortex* **17**, 951-961 (2007).
127. Watkins, K. E. et al. Structural Asymmetries in the Human Brain: a Voxel-based Statistical Analysis of 142 MRI Scans. *Cereb. Cortex* **11**, 868-877 (2001).
128. Luders, E., Gaser, C., Jancke, L. & Schlaug, G. A voxel-based approach to gray matter asymmetries. *Neuroimage* **22**, 656-64 (2004).

129. Toga, A. W. & Thompson, P. M. MAPPING BRAIN ASYMMETRY. *Nat Rev Neurosci* **4**, 37-48 (2003).
130. Dalton, K. M. et al. Gaze fixation and the neural circuitry of face processing in autism. *Nat Neurosci* **8**, 519-26 (2005).
131. Lundqvist, D., Flykt, A. & Ohman, A. Karolinska Directed Emotional Faces (Department of Neurosciences, Karolinska Hospital, Stockholm, Sweden). *Karolinska Directed Emotional Faces*, (Department of Neurosciences, Karolinska Hospital, Stockholm, Sweden) (1998).
132. Cox, R. W. AFNI: software for analysis and visualization of functional magnetic resonance neuroimages. *Comput.Biomed.Res.* **29**, 162-173 (1996).
133. Birn, R. M., Diamond, J. B., Smith, M. A. & Bandettini, P. A. Separating respiratory-variation-related fluctuations from neuronal-activity-related fluctuations in fMRI. *Neuroimage* **31**, 1536-48 (2006).
134. Reeves, A. G. *Epilepsy and the corpus callosum* (Plenum Press, New York, 1985).
135. Birn, R. M. & Bandettini, P. A. The effect of stimulus duty cycle and "off" duration on BOLD response linearity. *Neuroimage* **27**, 70-82 (2005).
136. Bandettini, P., Birn, R., Kelley, R. & Saad, Z. Dynamic nonlinearities in BOLD contrast: neuronal or hemodynamic? *Elsevier Excerpta Medica International Congress Series.* **1235**, 73-85 (2002).

Figure Legends:

Figure 1: Symmetric Template Formation

Figure 2: Visual Comparison of TIA Approaches Using an Unthresholded T-score Map

Figure 3: Visual Comparison of TIA Approaches Using an Unthresholded Difference in Z-scores Map (Autism-Control)

Figure 4: Visual Comparison of TIA Approaches Using a Map of Z-score Differences (Autism-Control) Thresholded at $t(22)=3.12$; $p=0.005$.

Symmetric Template Formation

Mean TLRC Brain + Mirrored TLRC Brain = Symmetric Template

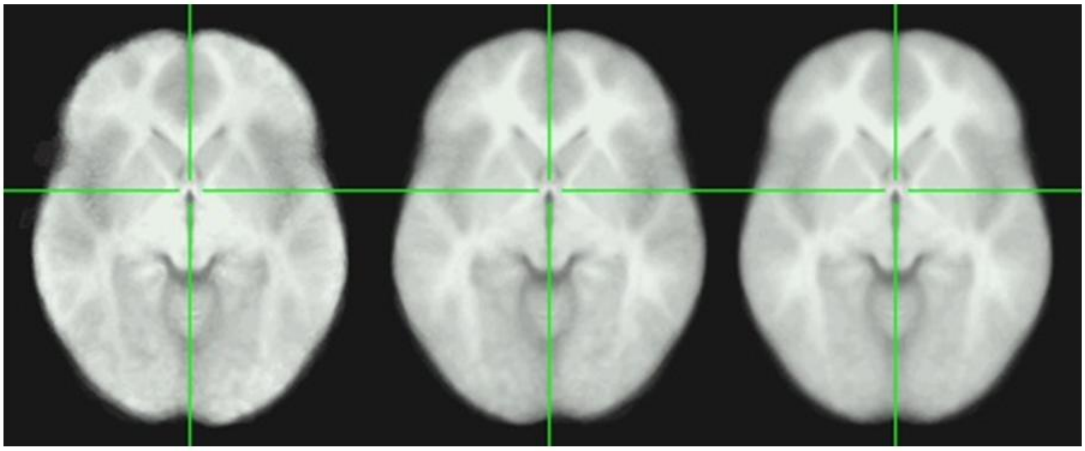

Right Left

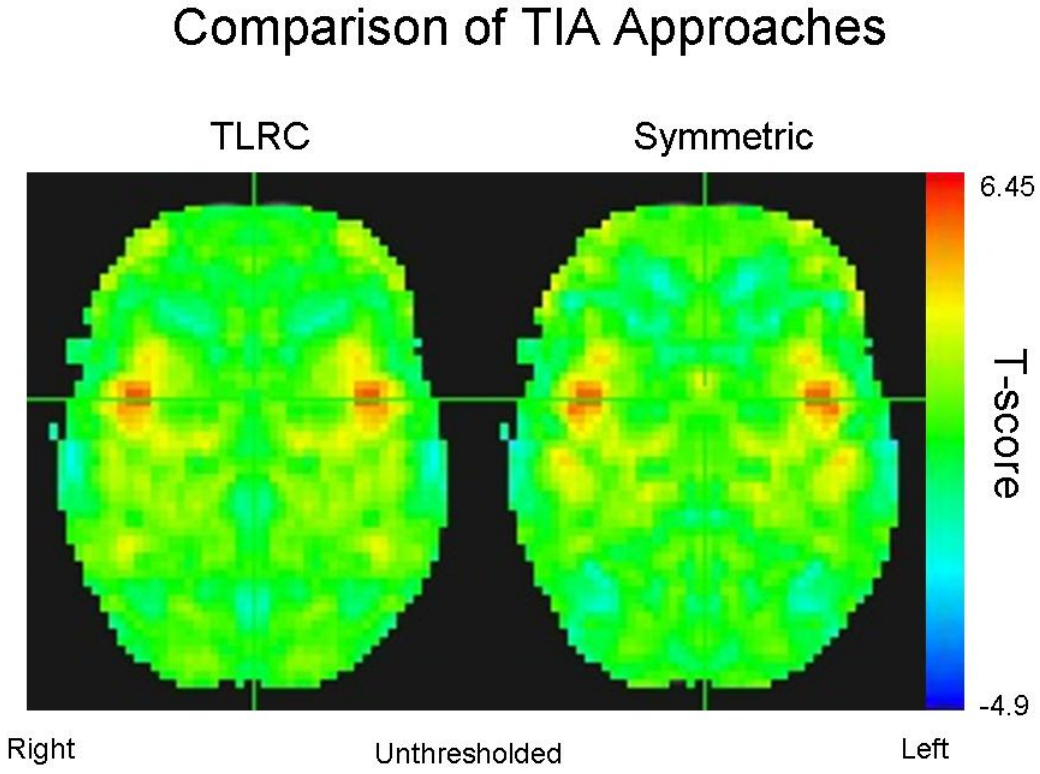
Comparison of TIA Approaches
TLRC
Symmetric
6.45
T-score
-4.9
Right
Unthresholded
Left

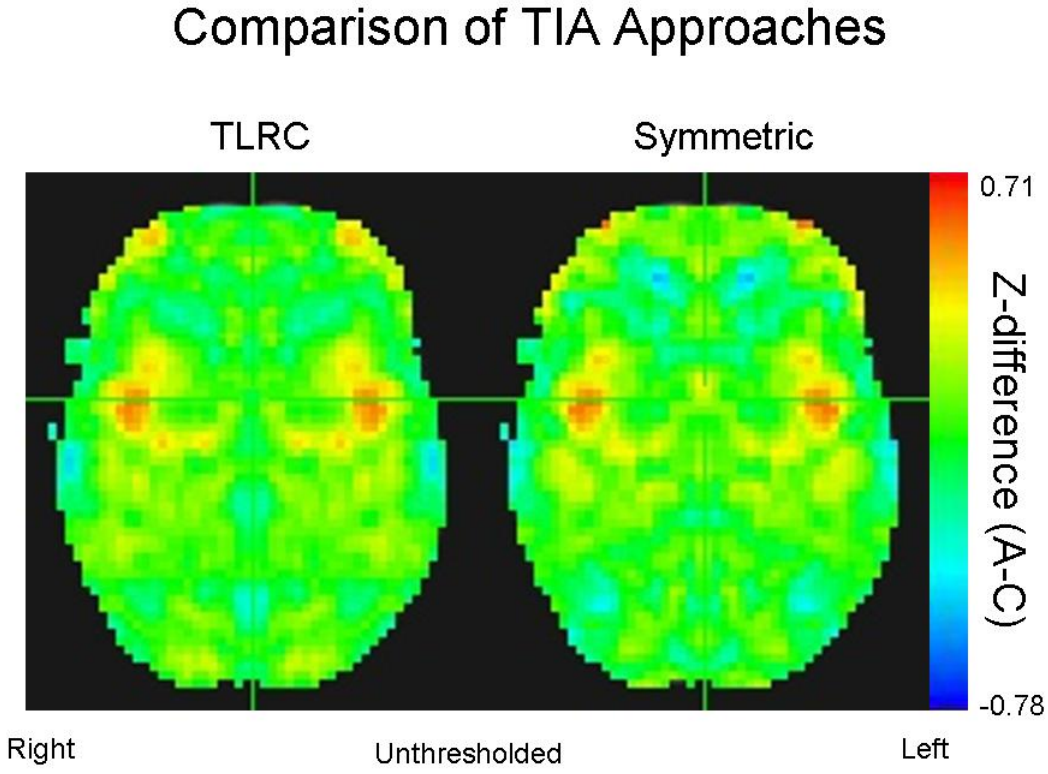
Comparison of TIA Approaches
TLRC
Symmetric
0.71
Z-difference (A-C)
-0.78
Right
Unthresholded
Left

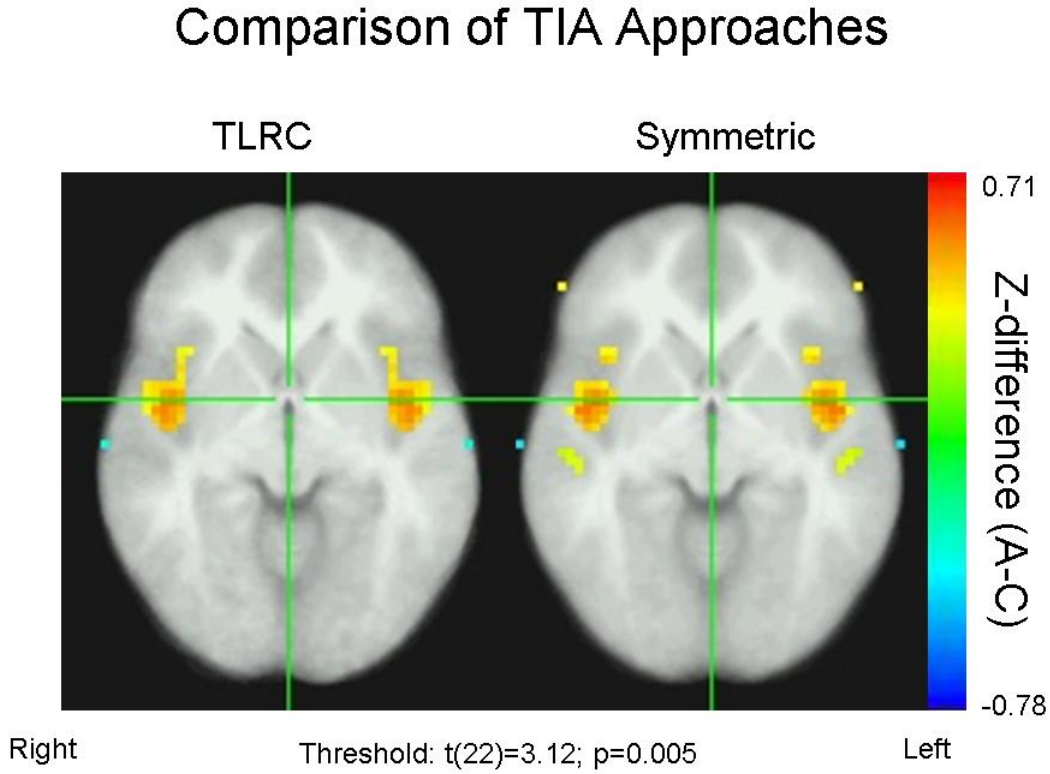
Comparison of TIA Approaches
TLRC
Symmetric
0.71
Z-difference (A-C)
-0.78
Right
Threshold: t(22)=3.12; p=0.005
Left

Appendix
On-line correlation Matlab code from page 22 [32].

```
% Calculating the on-line correlation coefficient CorrXY between two variables: an input
% variable X, and an output variable Y

SumX=0;
SumY=0;
SumXY=0;
SumX2=0;
SumY2=0;
CorrXY=[];

WHILE there are data pairs (x,y) from the input stream, DO
{
        INPUT the current data pair (x(i), y(i));

        SumX=SumX+x(i);
        SumY=SumY+y(i);
        AvX=SumX/i;
        AvY=SumY/i;
        SumXY=SumXY +(x(i)-AvX * (y(i)-AvY));
        SumX2=SumX2 + (x(i)-AvX)^2;
        SumY2=SumY2 + (y(i)-AvY)^2;
        the current value for the correlation coefficient is;
        CorrXY(i) = SumXY / sqrt(SumX2 * SumY2);
}
```

Wavelet correlation is possible using the WMTSA Wavelet Toolkit for MATLAB
http://www.atmos.washington.edu/~wmtsa/